SIAM J. Appl. Math.
Vol. 71, No. 6, pp. 2151–2167

GRAVITATIONAL OVERTURNING IN STRATIFIED PARTICULATE FLOWS*

YURI D. SOBRAL† AND E. JOHN HINCH‡

Abstract. With the motivation of understanding the formation of bubbles in fluidized beds, we investigate the stability of stratified particulate flows to transverse disturbances, leading to gravitational overturning. We consider a one-fluid model in which particles are responsible for the stratification of the flow but do not slip relative to the fluid and do not diffuse. A linear stability analysis and a numerical simulation of the governing equations are performed in order to determine and characterize the instability of the flow. We observe that stratified flows are unstable to transverse disturbances and that the instability is driven by a tilt-and-slide mechanism that creates ascending regions of low concentration of particles and descending regions of high concentration of particles. This mechanism might be related to the formation of bubbles in fluidized beds.

Key words. gravitational overturning, fluidized beds, bubble formation, secondary instability, concentration waves

AMS subject classifications. 76E99, 76D50, 76T20

DOI. 10.1137/100802426

1. Introduction.

The gravitational instability of stratified flows has been widely studied in the literature, mainly in the context of natural convection, where thermal gradients are responsible for the stratification of the flow [1]. Most of the works in this area have focused on flows confined between two horizontal boundaries, aiming to understand the heat transfer mechanisms from the surface of the Earth to the atmosphere, to understand the appearance of convective rolls, or even to extend these concepts to general atmosphere and ocean dynamics, with great focus on mixing and transition to turbulence. Nevertheless, for flows in unbounded domains in which particles are responsible for the stratification, it seems that the first stability study of the gravitational instability of stratified fluids was carried out in [2], inspired by the question of formation of bubbles in fluidized beds [3].

A fluidized bed is defined as follows. Consider the flow of a fluid through a bed of solid particles supported by a perforated plate. The flow is in the vertical upwards direction, against gravity. Before the flow rate reaches a critical value, the fluid flows through the particles as if they were a porous medium. The critical flow rate is the one at which the drag exerted on the particles by the flow balances their weight corrected for buoyancy. At this value, the flow rate is such that some particles become mobile and a very small expansion of the region occupied by the particles is observed. Any further increase in the flow causes the particles to become fully mobile and to occupy a larger region of the reservoir. The particles are then said to be fluidized, and the

*Received by the editors July 16, 2010; accepted for publication (in revised form) September 14, 2011; published electronically December 13, 2011.
http://www.siam.org/journals/siap/71-6/80242.html

†Department of Applied Mathematics and Theoretical Physics, Centre for Mathematical Sciences, University of Cambridge, Wilberforce Road, Cambridge, CB3 0WA, United Kingdom. Current address: Departamento de Matemática, Universidade de Brasília, Campus Universitário Darcy Ribeiro, 70910-900 Brasília-DF, Brazil (Y.D.Sobral@damtp.cam.ac.uk). This author was supported by the CAPES Foundation of the Ministry of Education of Brazil.

‡Department of Applied Mathematics and Theoretical Physics, Centre for Mathematical Sciences, University of Cambridge, Wilberforce Road, Cambridge, CB3 0WA, United Kingdom (E.J.Hinch@damtp.cam.ac.uk).

system is usually referred to as a fluidized bed. The name fluidized bed is due to the fact that the particles in this condition can be stirred and poured as a fluid [4, 5].

One of the most intriguing aspects of fluidization is its unstable behavior. In most cases of practical applications, it is very difficult to obtain a particulate fluidization, in which large gradients of concentration of particles on the scale of the fluidization reservoir are not present. In fact, large regions free of particles, usually called bubbles, are seen to propagate along the bed and are responsible for significant changes of the dynamics of the flow.

Many works have devoted attention to these instabilities in fluidized beds [6, 7, 8, 9, 10, 11, 12, 13]. The first works were carried out in a one-dimensional regime and observed that plane waves of concentration of particles of small amplitude were linearly unstable and would grow in time and in space. The occurrence of bubbles was then linked to these instabilities, but definitive evidence of this connection is still lacking [5].

In fact, when the geometry is confined to one dimension, the primary instabilities, as the one-dimensional waves of concentration of particles are often called, evolve into large-amplitude concentration waves, with well defined regions of high and low concentrations. However, during their evolution, and also when they reach a finite-amplitude steady state, these structures create in the fluidized bed a horizontally stratified configuration of heavier, i.e., more concentrated, fluid above light, i.e., less concentrated, fluid. In a bi- or tri-dimensional scenario, it is speculated [14] that the stratification generated by the unstable primary waves would suffer a gravitational instability, setting up the conditions for the formation of bubbles. The gravitational overturning would cause the more concentrated regions to fall over the less concentrated regions, in analogy to the heavy over light instability, and eventually trigger nonlinear processes that lead to the formation of an ascending low-concentration structure, which ultimately evolves into a bubble. It is not yet clear how the region of low concentration evolves to a region empty of particles, although recent studies [10, 14, 15, 16] indicate that there is a larger flux of particles leaving the low-concentration structure via its lower surface than of particles entering via its upper surface.

Following the works in [2, 3], a stability analysis of a stratified fluid in an unbounded infinite domain will be performed in this work. The main assumption is that the stratification, due to the presence of particles in the fluid at different local concentrations, is responsible for variations in the local value of the density of the fluid and that those particles do not have a motion of their own; i.e., the mixture of particles and fluid behaves as one single bulk continuum. This can be understood as the limiting case of very low Stokes number regime, in which the particles have no inertia and, therefore, no relative motion with respect to the fluid. Furthermore, we focus on the large scale instabilities that might lead to the formation of bubbles in fluidized beds, and therefore hydrodynamical interactions among particles and the resulting changes on the fluid microstructure, such as a viscosity depending on the particle concentration, are not considered. Although real fluidized beds cannot be modelled as the idealized continuum mixtures outlined here, since the relative velocity between the particles and the fluid is considerable, some important physical insight into the mechanics of gravitational overturning can be gained from an investigation of the unstable behavior of stratified flows [2].

In a future paper, we hope to investigate the gravitational overturning instability in a two-fluid model of a fluidized bed. We will be interested in comparing predictions of the growth rate of the linearized disturbances, as well as comparing the nonlinear development. To aid this future comparison, we will nondimensionalize the one-fluid

model of this paper with three key parameters of the two-fluid model: the terminal velocity v_t of the particles, a factor β_0, and a certain length scale L, which are absent in the one-fluid model. Unsurprisingly, we shall find that the dimensional growth rates predicted in this paper are independent of these parameters.

2. Governing equations.

2.1. The Navier–Stokes equation and the Boussinesq approximation.

Consider an infinite domain filled with a mixture of fluid of density ρ_f and particles of density ρ_p. The particles are present at a local volume concentration ϕ, and gravity is acting vertically downwards, in the direction of the negative z-axis. The local density of this mixture is therefore given by

$$\rho = \rho_f(1-\phi) + \rho_p\phi. \tag{2.1}$$

The viscosity of the mixture is μ, and we assume that it does not depend on the concentration of particles. In fact, since the focus of the present work is on the linearized regime, we assume that the viscosity of the mixture does not depend on the concentration of the particles. In nonlinear regimes, the viscosity of the bulk should depend on the local concentration of particles and would change the time scales of dissipation in the flow and, consequently, the time scale of the instabilities. In addition, the concentration of particles is normally very high in real fluidized beds, and the choice of an appropriate dependence of the viscosity as a function of the concentration of particles would be very difficult. Note that this problem is different from the determination of the viscosity of the particulate phase in the two-fluid model, as discussed in [7].

The governing equation of the motion of the mixture is the Navier–Stokes equation,

$$\rho\left(\frac{\partial \mathbf{w}}{\partial t} + \mathbf{w}\cdot\nabla\mathbf{w}\right) = -\nabla p + \mu\nabla^2\mathbf{w} + \rho\mathbf{g}, \tag{2.2}$$

where $\mathbf{w}$ denotes the velocity, p the pressure, and $\mathbf{g}$ the acceleration of gravity, and we also assume that the mixture is incompressible; that is,

$$\nabla\cdot\mathbf{w} = 0. \tag{2.3}$$

The changes in the density of the flow are due to local changes in the concentration of the particles. Since the quantity of particles in the flow is conserved, the local concentration ϕ obeys a conservation law. Assuming that the particles are just convected by the fluid and do not diffuse, as opposed to the work in [2], we obtain the following equation for the local concentration of particles:

$$\frac{\partial\phi}{\partial t} + \nabla\cdot(\phi\mathbf{w}) = 0. \tag{2.4}$$

We now seek dimensionless forms of (2.2), (2.3), and (2.4). Inspired by the fluidization problem, and to make possible a comparison of the results obtained here with the two-fluid theory, the scale for the velocity is chosen to be the terminal velocity of the particles, v_t, and therefore the time scale is given directly by L/v_t, with L a length scale. With the same motivation, we take as the length scale that set by the viscous dissipation and by the drag on the particulate phase of a fluidized bed. In fact, in the two-phase model of fluidized beds, the particles are considered to be a

continuum viscous phase that interacts with the fluid phase through a (drag) force that is very often considered to be linear with respect to the relative velocities of the phases. A detailed account for the origin of this force can be found in [17]. The choices of scales made here are sufficient to make the study carried out in this work compatible with works on the stability of fluidized beds using the standard two-fluid formulation. Therefore, we set

$$L = \sqrt{\frac{v_t \mu}{(\rho_p - \rho_f) g \beta_o}}. \tag{2.5}$$

Also, in (2.5), β_o is defined as

$$\beta_o = \frac{\phi_o}{(1-\phi_o)^n}, \tag{2.6}$$

which is the drag coefficient of the fluid-particle interaction force that appears in the standard two-fluid formulation of fluidized beds [6]. We then can write (2.2) as

$$\beta_0 Re \left(\frac{\partial \mathbf{w}}{\partial t} + \mathbf{w} \cdot \nabla \mathbf{w} \right) = -\nabla p + \beta_0 \nabla^2 \mathbf{w} - \phi \mathbf{e}_z. \tag{2.7}$$

The dimensionless parameter in (2.7) is the Reynolds number defined as

$$Re = \frac{\rho_0 v_t L}{\mu}, \tag{2.8}$$

with $\rho_0 = \rho_f(1-\phi_0) + \rho_p \phi_0$ being the density of the mixture calculated at the homogeneous state ϕ_0. Note that the Boussinesq approximation allows us to assume that $\rho \approx \rho_o$ on the left-hand side of (2.2). This means that the density variations are important to the dynamics only via their effect on the gravitational terms (buoyancy), not via the inertia of the flow. In addition, we make a further simplification by ignoring the z-dependence of ρ_o, setting it to a constant value calculated at the homogeneous concentration ϕ_o. In addition, the continuity equation, (2.3), and the particle conservation equation, (2.4), keep their form when made dimensionless.

We should remark here that our nondimensionalization of the one-fluid model of a fluidized bed used in this paper uses the parameters v_t, β_0, and L from the two-fluid model. These parameters are used in order to simplify comparisons between the predictions of the two models in a future paper.

We now propose that the pressure p is perturbed around its equilibrium value $p_o = p_o(z)$,

$$p = p_o + p', \tag{2.9}$$

with the prime denoting a deviation from the equilibrium state. We also note that the variations of the density of the fluid are due to the presence of particles at different local concentrations. We define the perturbation of the concentration of particles as

$$\phi = \phi^*(z) + \phi', \tag{2.10}$$

where $\phi^*(z) = \phi_o + \phi_1(z)$, with ϕ_o denoting the homogeneous concentration of particles in the undisturbed state and $\phi_1(z)$ the initial stratification of the flow. For the equilibrium state, $\nabla p_o = \phi_0$, so that a first simplified version of (2.7) is given by

$$\left(\frac{\partial \mathbf{w}}{\partial t} + \mathbf{w} \cdot \nabla \mathbf{w} \right) = -\nabla p' + \mu \nabla^2 \mathbf{w} + \rho' \mathbf{g}. \tag{2.11}$$

Finally, we note that the mixture has its velocity field $\mathbf{w}_o$ disturbed as well,

$$\mathbf{w} = \mathbf{w}_o + \mathbf{w}', \tag{2.12}$$

with $\mathbf{w}_o = q\mathbf{e}_z$ remaining constant throughout the motion. The flow rate q is given by [11, 18]

$$q = (1 - \phi_o)^n, \tag{2.13}$$

where $n = 3$ is an experimental coefficient. Therefore, the linear terms $\mathbf{w}_o \cdot \nabla \mathbf{w}'$ in the linearized (2.11) and $\mathbf{w}_o \cdot \nabla \phi'$ in the linearized (2.4) represent the translation of the disturbances with velocity $q\mathbf{e}_z$ that disappear from the equation when we change to a frame of reference moving with the same velocity.

Dropping the primes for the perturbations, the final linear equations governing the dynamics of the stratified flows that we consider in this study are the momentum equation,

$$\beta_0 Re \frac{\partial \mathbf{w}}{\partial t} = -\nabla p + \beta_0 \nabla^2 \mathbf{w} - \phi \mathbf{e}_z, \tag{2.14}$$

the continuity equation, (2.3), and the linearized particle conservation equation,

$$\frac{\partial \phi}{\partial t} + \mathbf{w} \cdot \nabla \phi_1 = 0. \tag{2.15}$$

Note that (2.15) is obtained taking into account the incompressibility of the flow, (2.3).

3. Stability of stratified horizontal layers.

3.1. The case without inertia. We will initially restrict ourselves to the inertia-free case, i.e., $Re = 0$ in (2.14).

The stability analysis will be performed with respect to the base state of vertical stratification. Assume that z denotes the vertical direction and that x denotes the horizontal direction. Therefore, the base state of this flow is defined as

$$\phi_{\text{base state}} = \phi_o + \varepsilon_1 \sin(\kappa z), \tag{3.1}$$

where ε_1 is the amplitude of the vertical stratification with wavelength κ.

We now propose the disturbances of the concentration of particles and of the vertical velocity w_z to be of the form

$$\phi = \mathcal{F}(z) \exp(\zeta t) \sin(\ell x), \tag{3.2}$$

$$w_z = \mathcal{W}(z) \exp(\zeta t) \sin(\ell x), \tag{3.3}$$

where $\mathcal{F}(z)$ and $\mathcal{W}(z)$ are the amplitude functions, ζ is the temporal growth rate of these disturbances, and ℓ is their horizontal wave number.

From (2.3), the disturbance of the horizontal velocity of the flow, w_x, can be readily found to be

$$w_x = \frac{D\mathcal{W}(z)}{\ell} \exp(\zeta t) \cos(\ell x), \tag{3.4}$$

where D denotes a differentiation with respect to z. Similarly, from the x-component of (2.7), the pressure disturbances can be obtained:

$$p = \frac{\beta_o}{\ell^2} \exp(\zeta t) \sin(\ell x) \left[\mu \left(D^2 - \ell^2\right)\right] D\mathcal{W}(z). \tag{3.5}$$

Now, using (3.4) and (3.5) in the z-component of (2.14), we have

$$\beta_o \left(D^2 - \ell^2\right) \left[\mu \left(D^2 - \ell^2\right)\right] \mathcal{W}(z) + \ell^2 \mathcal{F}(z) = 0. \tag{3.6}$$

The conservation of particles now reads

$$\mathcal{F}(z)\zeta + \mathcal{W}(z)\varepsilon_1 \cos(\kappa z) = 0, \tag{3.7}$$

so that, when combined with (3.6), the following equation for the amplitude of the disturbances of the vertical velocity w_z is obtained:

$$\left(D^2 - \ell^2\right)^2 \mathcal{W}(z) - \frac{\varepsilon_1 \kappa \ell^2}{\beta_o \zeta} \cos(\kappa z) \mathcal{W}(z) = 0. \tag{3.8}$$

The growth rates ζ of the transverse modes ℓ will be found from the solutions of the equation above.

3.1.1. Approximate analytical solutions for the problem without inertia. Proposing a series expansion in terms of cosines for $\mathcal{W}(z)$,

$$\mathcal{W}(z) = \sum_{m=0}^{M} s_m \cos(m\kappa z), \tag{3.9}$$

and substituting (3.9) into (3.8), we obtain

$$\sum_{m=0}^{M} s_m \left\{ \left[(\kappa m)^2 + \ell^2\right]^2 \cos(m\kappa z) - \frac{\ell^2}{2\mathcal{A}} \left[\cos\Big((m-1)\kappa z\Big) + \cos\Big((m+1)\kappa z\Big)\right] \right\} = 0, \tag{3.10}$$

where

$$\mathcal{A} = \frac{\beta_o \zeta}{\varepsilon_1 \kappa} \tag{3.11}$$

is a modified growth rate. Equation (3.10) yields a system of equations relating the coefficients $s_0, \ldots, s_M$ and ζ. An approximate solution for the modified growth rate $\mathcal{A}$ can be found by truncating the system in (3.10) at a given M.

The simplest approximation is obtained by setting $M = 1$, from which $\mathcal{A}$ is found to be

$$\mathcal{A} = \frac{\pm 1}{\sqrt{2}\left(\kappa^2 + \ell^2\right)}. \tag{3.12}$$

Similarly, truncating at $M = 2$ gives

$$\mathcal{A} = \frac{\pm 1}{\sqrt{2}\left(\kappa^2 + \ell^2\right)} \sqrt{1 + \frac{\ell^4}{\left(4\kappa^2 + \ell^2\right)^2}}. \tag{3.13}$$

Finally, truncating at $M = 3$, the solution of the system in (3.10) gives an algebraic biquadratic equation:

$$\begin{aligned} \frac{\ell^4}{\left(9\kappa^2 + \ell^2\right)^2} - 2 \left[\ell^4 + 2\left(4\kappa^2 + \ell^2\right)^2 + \frac{\ell^4 \left(\kappa^2 + \ell^2\right)^2}{\left(9\kappa^2 + \ell^2\right)^2}\right] \mathcal{A}^2 \\ + 8\left(\kappa^2 + \ell^2\right)^2 \left(4\kappa^2 + \ell^2\right)^2 \mathcal{A}^4 = 0. \end{aligned} \tag{3.14}$$

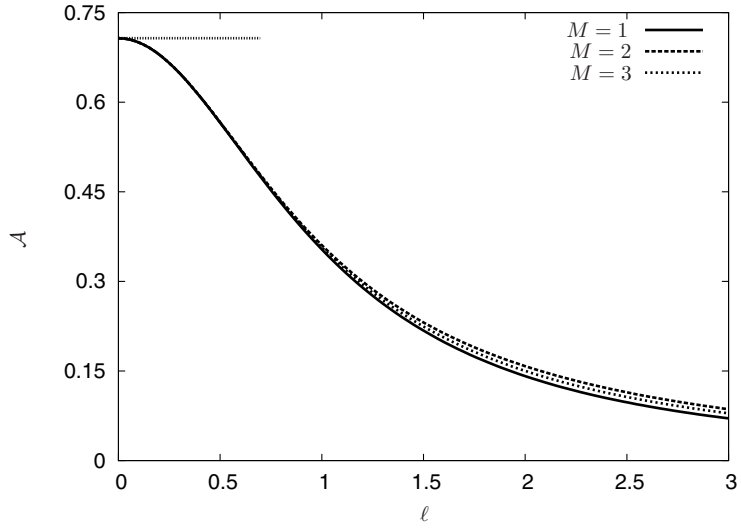

FIG. 1. *Convergence of the modified growth rates $\mathcal{A}$ with respect to the truncation of the approximation in* (3.9). *Results obtained for $\kappa = 1$. The horizontal line represents the $\ell \to 0$ behavior of the growth rates from* (3.15).

Despite the fact that (3.14) can be easily solved explicitly for $\mathcal{A}$, the resulting expression is too complicated and would not add much to the analyses that follow. Truncations at higher orders will give more accurate estimates but more complicated expressions for $\mathcal{A}$.

The convergence of the growth rates with respect to the order of the truncation, the parameter M in (3.10), is presented in Figure 1. The growth rates of the small wave number waves is correctly calculated with the very simple approximation for $M = 1$, although those for large ℓ are sensitive to the truncation order and would require higher order for a precise estimate. The good convergence of the growth rates for $M = 3$ will be confirmed later by numerical methods in section 3.1.2.

Note that the positive root for $\mathcal{A}^2$ resulting from (3.14) is the relevant one for obtaining the growth rate ζ and is plotted in Figure 1. We observe that the growth rate decreases with the wave number ℓ; that is, short waves are less unstable than long waves. Therefore, one should expect that the horizontal disturbances that will be observed are the large scale ones. However, the growth rates for very small wave numbers are very similar, indicating that more than one mode might naturally dominate the dynamics of real systems.

Also in Figure 1, one can see that the unstable disturbances do not become stable at large wave numbers. This is due to the absence of particle diffusion in the particle conservation equation, (2.4). This mechanism was considered in [2], and they observed a short wavelength cutoff on the growth rates.

Additionally, it should be noted in Figure 1 that the growth rates do not tend to zero as $\ell \to 0$. In fact, from (3.12) the $\ell \to 0$ limit can be calculated explicitly and is given by

$$\mathcal{A} \approx \pm \frac{1}{\sqrt{2}\kappa^2}, \tag{3.15}$$

the same obtained by the higher-order truncations in (3.13) and (3.14). This value

is plotted in Figure 1 as the fine dotted horizontal line. On the other hand, if $\ell = 0$, there is no horizontal variation in the concentration, so this perturbation is stable, $\mathcal{A} = 0$. In fact, $\mathcal{A}$ is discontinuous at $\ell = 0$ due to the absence of inertia on these calculations, as will be seen in section 3.2.

The dimensional value of the growth rate in (3.15) is

$$\zeta_{\text{dimensional}} = \frac{1}{\sqrt{2}} \frac{\Delta\rho g \varepsilon_1}{\mu \kappa_d}, \tag{3.16}$$

where κ_d is the dimensional vertical wave number of the base state. Note, as expected, that this dimensional growth rate does not depend on the parameters v_t and β_0 introduced in the nondimensionalization. The larger the stratification, i.e., the larger the value of ε_1, the faster the gravitational instabilities grow. This is in agreement with observations in fluidized beds [4, 5] that bubbles are more frequently observed in gas-fluidized beds. In these systems, in which the fluid and the particles have a considerable difference in density, the growth rates of the primary instabilities are then much larger than in liquid-fluidized beds. As the stratification in fluidized beds originates from the primary instabilities, the gravitational overturning, as predicted in this work, is more likely to occur in gas-fluidized beds.

3.1.2. Numerical solutions of the eigenvalues for the problem without inertia. The growth rates of the transverse modes have also been found numerically. This was carried out by discretizing (3.8) using a second-order finite-difference scheme and calculating the eigenvalues of the coefficient matrix resulting from the discretization process. The idea of using this method was to verify that the choice of the truncation was adequate or to see whether more terms would be necessary to determine correctly the growth rates of the disturbances.

Using the parameter $\mathcal{A}$ as defined in (3.11) and approximating the derivatives with respect to z in (3.8) by a second-order finite-differences scheme, we obtain

$$\mathcal{W}_{i+2} - b\mathcal{W}_{i+1} + (a + a_i)\mathcal{W}_i - b\mathcal{W}_{i-1} + \mathcal{W}_{i-2} = 0, \tag{3.17}$$

where $\mathcal{W}_i$ denotes the value of $\mathcal{W}$ at the node i of the discretized grid and Δz denotes the space step of the discretized mesh of N_z points. The coefficients a, b, and a_i are given, respectively, by

$$a = 6 + 4\ell^2(\Delta z)^2 + \ell^4(\Delta z)^4, \quad b = 4 + 2\ell^2(\Delta z)^2, \quad a_i = -\frac{\ell^2(\Delta z)^4}{\mathcal{A}} \cos(\kappa z_i). \tag{3.18}$$

We use N_z points to discretize one wavelength $2\pi/\kappa$ of the disturbance, and impose periodic boundary conditions, so that (3.17) is well defined for every node i in the range of integers $[0, N_z - 1]$.

The eigenvalues of the matrix of the coefficients of (3.17) will approach the growth rates for the transverse instabilities for large N_z. Before writing the eigenvalue problem for the discretized problem in matrix form, we can split a_i in (3.18) into two terms, a constant part composed of the first three terms on the right-hand side of (3.18), and another part containing the modified eigenvalue $\mathcal{A}$, that is, the last term on the right-hand side of (3.18). This allows us to write (3.17) in the following matrix form:

$$\tilde{\mathbb{A}}\mathbb{W} = \mathcal{A}^{-1}\left(\mathbb{I} + \mathbb{A}\right)\mathbb{W}, \tag{3.19}$$

where

$$\tilde{\mathbb{A}} = \begin{bmatrix} a & b & 1 & 0 & 0 & \cdots & 0 & 0 & 0 & 1 & b \\ b & a & b & 1 & 0 & \cdots & 0 & 0 & 0 & 0 & 1 \\ 1 & b & a & b & 1 & \cdots & 0 & 0 & 0 & 0 & 0 \\ 0 & 1 & b & a & b & \cdots & 0 & 0 & 0 & 0 & 0 \\ \vdots & \vdots & \vdots & \vdots & \vdots & \ddots & \vdots & \vdots & \vdots & \vdots & \vdots \\ 0 & 0 & 0 & 0 & 0 & \cdots & b & a & b & 1 & 0 \\ 0 & 0 & 0 & 0 & 0 & \cdots & 1 & b & a & b & 1 \\ 1 & 0 & 0 & 0 & 0 & \cdots & 0 & 1 & b & a & b \\ b & 1 & 0 & 0 & 0 & \cdots & 0 & 0 & 1 & b & a \end{bmatrix}, \tag{3.20}$$

and where $\mathbb{W}$ is the column matrix with the $\mathbb{W}_i$ for $i = 0, \ldots, N-1$. Also in (3.19), $\mathbb{I}$ denotes the identity matrix and $\mathbb{A}$ is a diagonal matrix such that $[\mathbb{A}]_{ii} = \mathcal{A}a_i$ for $i = 0, \ldots, N-1$ and $[\mathbb{A}]_{ij} = 0, i \neq j$. Therefore, we observe that the discretized version of the gravitational stability problem of stratified flows in (3.19) is a generalized eigenvalue problem. We used a subroutine of the library LAPACK to solve (3.19) for the modified eigenvalues $\mathcal{A}$.

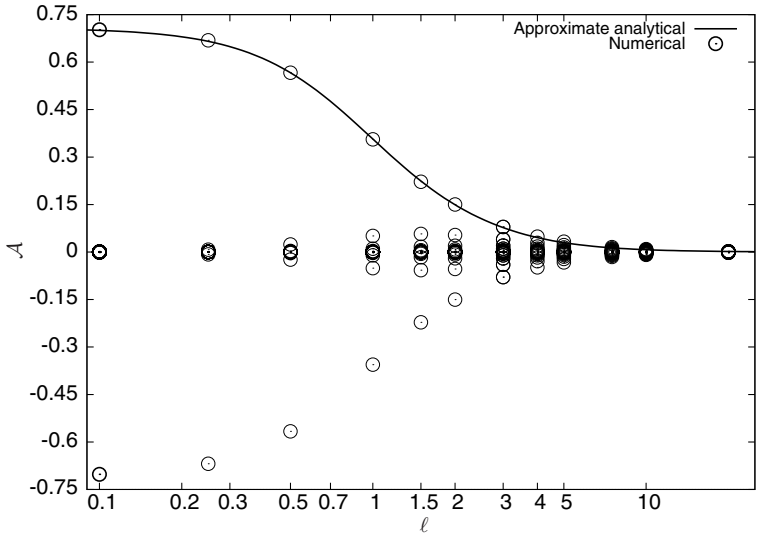

FIG. 2. *Comparison of the solutions obtained via the analytical and the numerical methods. Line: growth rates calculated using the solution of* (3.14). *Points: eigenvalues of the discrete problem in* (3.19). *Results obtained for* $N_z = 550$ *and* $\kappa = 1$.

Figure 2 shows the results obtained for $\mathcal{A}$ from the approximate analytical solution, presented in (3.14), and the numerical calculation for the discretized problem, (3.19). It is observed that the approximate analytical results obtained for a truncation of four terms, i.e., $M = 3$, are in very good agreement with the results obtained from the numerical results. We note that the numerical method provides, for each ℓ, N_z eigenvalues of the generalized problem in (3.19), but the largest positive one, which numerically can occur with multiplicity, is the relevant one, given analytically by (3.14).

3.2. Approximate analytical solutions for the problem with inertia. In this case, we have to consider (2.14) in its full form. The procedure for obtaining a

governing equation in terms of the amplitude of the velocity disturbances described in section 3.1 is repeated here, and we obtain

$$\zeta\left(D^2-\ell^2\right)^2\mathcal{W}(z)-\frac{\varepsilon_1\kappa\ell^2}{\beta_o}\cos(\kappa z)\mathcal{W}(z)-\frac{Re\zeta^2}{1}\left(D^2-\ell^2\right)\mathcal{W}(z)=0. \tag{3.21}$$

We note that (3.21) is very similar to (3.8), with the exception of the last term on the left-hand side, which makes the dependence on ζ quadratic.

Similarly to the case $Re=0$, we propose a solution of the form of a series of cosines, as in (3.9), and substituting it into (3.21), the following equation is obtained:

$$\begin{aligned}\sum_{m=0}^{M} s_m\Bigg\{\Big\{\left[(\kappa m)^2+\ell^2\right]^2+\mathcal{AB}\left[(\kappa m)^2+\ell^2\right]\Big\}\cos(m\kappa z)\\ -\frac{\ell^2}{2\mathcal{A}}\Big[\cos\Big((m-1)\kappa z\Big)+\cos\Big((m+1)\kappa z\Big)\Big]\Bigg\}=0,\end{aligned} \tag{3.22}$$

where $\mathcal{A}$ is given by (3.11) and $\mathcal{B}$, a modified inertial parameter, is defined as

$$\mathcal{B}=\frac{\varepsilon_1\kappa Re}{\beta_o}. \tag{3.23}$$

We start by truncating at $M=1$ and find that $\mathcal{A}$ is the solution of the following incomplete fourth-order algebraic equation:

$$2\mathcal{B}^2\mathcal{A}^4+2\left[\Big(\kappa^2+\ell^2\Big)+\ell^2\right]\mathcal{BA}^3+2\ell^2\Big(\kappa^2+\ell^2\Big)\mathcal{A}^2-\frac{\ell^2}{\kappa^2+\ell^2}=0, \tag{3.24}$$

which is a not simple formula. Nevertheless, from (3.24) the $Re\to 0$ limit is observed to be consistent with (3.12) obtained for $Re=0$ and $M=1$. On the other hand, the $\ell\to 0$ limit cannot be inferred easily without an explicit solution for $\mathcal{A}$. Due to these difficulties, we opted to solve the system in (3.22) numerically for ζ, taking $M=3$ as for the case $Re=0$. The results are presented in Figure 3.

Figure 3 reveals that for large wave numbers the stability of the disturbances is not affected by inertia. Only for very small wave numbers is the growth of the disturbances reduced considerably. This is due to the fact that it takes longer to accelerate the larger fluid masses in long wavelength disturbances, and therefore their growth rates are reduced. In addition, we observe now that ζ is continuous at $\ell=0$.

4. Simulations of horizontally stratified flows. In this section, we will solve the full nonlinear equations governing the gravitational instability of particulate flows in order to check the linear stability results and evaluate how far the theory discussed in the previous section can be used. Also, we investigate whether there are nonlinear features in the evolution of the gravitational instability that can be captured by the model presented in this work.

4.1. Brief description of the numerical method. Throughout this section, we have used the indices x and z to identify the horizontal x- and the vertical z-components of a vector quantity, and the indices ij to denote the point on the discretized xz domain where a given property is being evaluated.

The system of equations (2.3), (2.4), and (2.11) was solved numerically using a primitive variables formulation and a pressure projection routine, in a code that used a second-order finite-differences scheme on a staggered grid with a forward Euler temporal scheme for time-stepping.

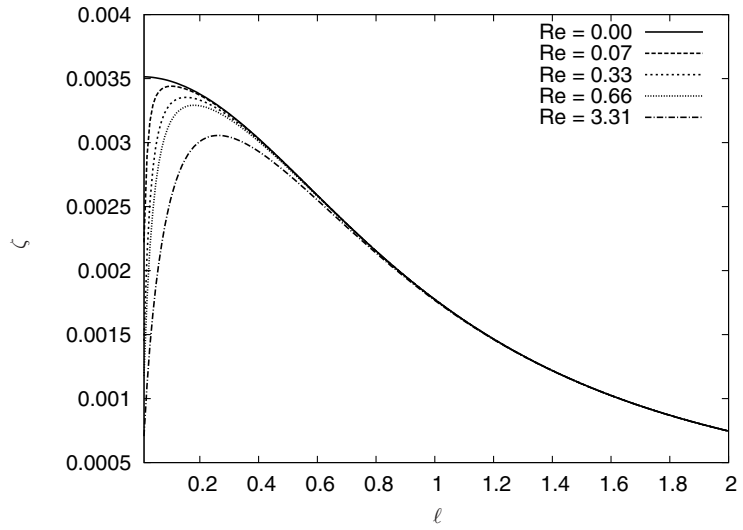

FIG. 3. *Growth rates for different values of Re obtained from the solution of* (3.22) *for* $M = 3$. *Results obtained for* $\kappa = 1$, $\phi_o = 0.55$, *and* $\varepsilon_1 = 0.03$.

The simulations were all carried out in a fully periodic rectangular grid, so periodic boundary conditions were imposed on all the variables, with the exception of the vertical pressure gradient, which had to account for the hydrostatic pressure in the bed. The initial conditions, in principle, are those that connect the flow studied here to the one-dimensional homogeneous state of fluidization [6], but now in this case considering only one bulk fluid in motion. However, when the trivial initial conditions of the perturbed homogeneous state were used, numerical oscillations in the initial transient of the calculation were observed in the simulations. This was considerably improved after a first-order correction, calculated from the analyses in section 3, was introduced in the initial conditions. Assuming the disturbances of particle concentration and of vertical velocity to be given by (3.2) and (3.3), respectively, and using (3.4), (3.5), (3.7), and the approximation in (3.9) for $\mathcal{W}(z)$, truncated at $M = 1$, the following corrected initial conditions are obtained for this problem:

$$\phi(t=0) = \phi_o + \varepsilon_1 \sin(\kappa z) + \varepsilon_2 \left(\ell^2 + \sqrt{2}\left(\ell^2 + \kappa^2\right)\cos(\kappa z)\right)\sin(\ell x), \tag{4.1}$$

$$w_x(t=0) = \frac{\varepsilon_2 \sqrt{2}\ell\kappa}{\beta_o\left(\ell^2 + \kappa^2\right)}\sin(\kappa z)\cos(\ell x), \tag{4.2}$$

$$w_z(t=0) = q - \frac{\varepsilon_2}{\beta_o}\left(1 + \frac{\sqrt{2}\ell^2}{\ell^2 + \kappa^2}\cos(\kappa z)\right)\sin(\ell x). \tag{4.3}$$

It should be noted that the velocities of the bulk have no corrections associated with the primary waves. We used a discrete two-dimensional Fourier transform to calculate the amplitude of the mode ℓ in the ℓ-κ space.

First-order accuracy in time and second-order accuracy in space of the code were checked thoroughly, and we also checked that the method is accurate when compared to the predictions of the linear theory. The growth rates of very small-amplitude modes were calculated from the simulations and are plotted in Figure 4, where the results from (3.22) for $M = 3$ are also plotted. We observe a very good agreement

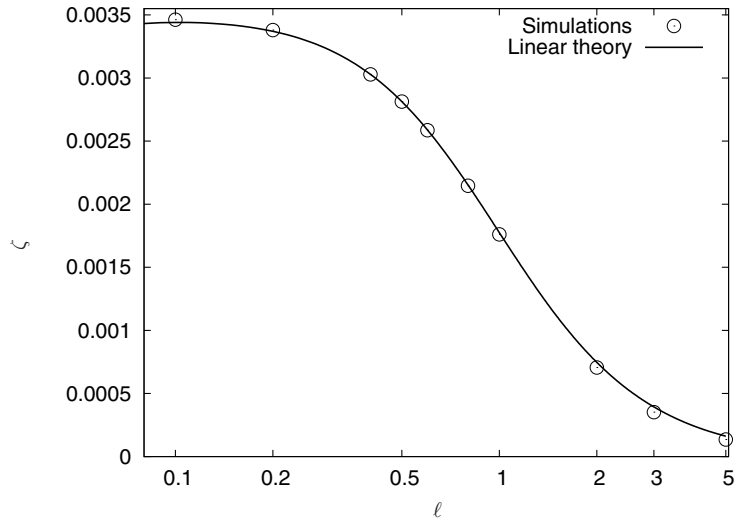

FIG. 4. *Growth rates of the secondary instability calculated from the simulations for small-amplitude modes, compared with the prediction of the linear theory. Results obtained for* $\kappa = 1$, $\phi_o = 0.55$, $Re = 0.07$, $\varepsilon_1 = 0.03$, *and* $\varepsilon_2 = 0.0005$.

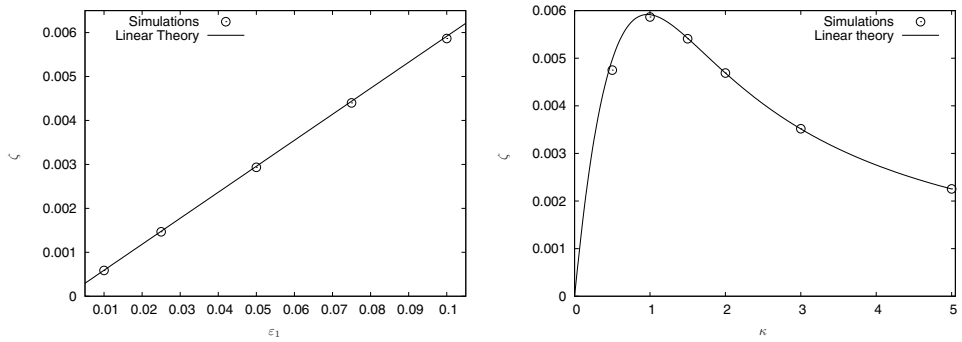

FIG. 5. *Growth rates of the secondary instabilities.* (a) *Influence of* ε_1, *obtained for* $\phi_o = 0.55$, $\kappa = 1$, *and* $\ell = 1$. (b) *Influence of the wave number* κ, *obtained for* $\phi_o = 0.55$, $\varepsilon_1 = 0.001$, *and* $\ell = 1$. *Other parameters are* $\varepsilon_2 = 0.0005$ *and* $Re = 0.07$.

of both methods of calculation. The growth rates of the short wavelength seem to be overestimated by the theory due to truncation effects.

4.2. Results of the numerical simulations in the linear regime. In this section, we present some results obtained in the linear regime of the secondary instabilities and the influence of the physical parameters on the growth of these instabilities.

The influence of the amplitude of the initial stratification ε_1 on the growth rates of the secondary instabilities is presented in Figure 5(a). The growth rates increase linearly with the amplitude of the initial stratification, as predicted by the linear theory. However, not only the amplitude of the initial stratification but also its wave number can influence the evolution of the secondary instabilities. Figure 5(b) shows that there is wave number of the initial stratification for which the secondary

instability will grow the fastest, similar to the prediction of the linear stability of the one-dimensional instabilities [6]. For the particular choice of parameters in Figure 5, $\kappa \approx 1$ is the most gravitationally unstable wavelength of the stratification.

The linear regime seems to dominate for a long time the growth of the secondary instabilities in the flows, as observed in Figure 6. For the simulation presented there, the linear theory gives $\zeta = 0.0005512$, and the comparison between the exponential growth predicted by the linear theory and the full numerical simulation indicates a good agreement up to times of around $t = 1000$. After this time, nonlinear inertial mechanisms start to become important, and the growth of the instabilities becomes slower than predicted by the linear theory.

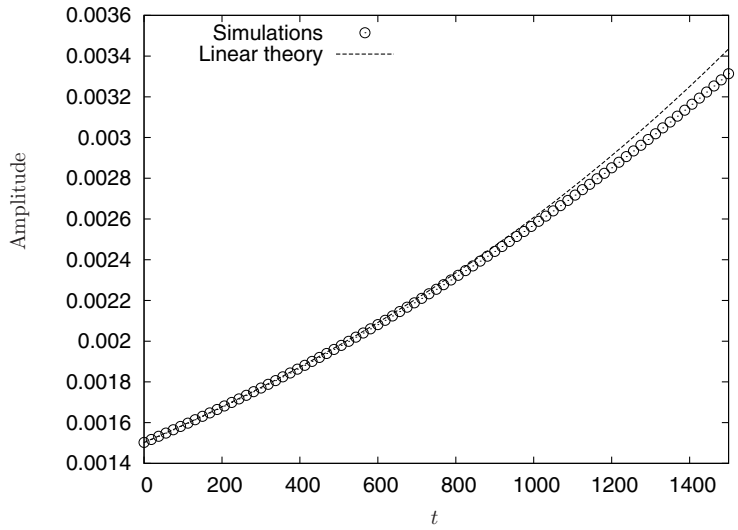

FIG. 6. *Amplitude of the secondary instability as a function of time. Results obtained for* $\ell = 0.25$, $\kappa = 1$, $\varepsilon_1 = 0.005$, $\varepsilon_2 = 0.001$, $Re = 0.07$.

Some snapshots of the evolution of a disturbance with $\ell = 0.25$ and $\kappa = 1$ can be seen in Figure 7. We observe that the layers of more concentrated and less concentrated regions tilt relative to one other as the instability evolves, indicating the unstable behavior of the initial stratification. This is compatible with the tilting of the horizontal layers described in [2].

The amplitude of the secondary instability presented in Figure 7 roughly only doubled in the time range investigated. Note that the range of the particle concentrations observed in all the snapshots presented in Figure 7 does not change. This indicates that the secondary instability is a configurational instability with no change in the range of concentration variations, as opposed to the slower primary instability in fluidized beds, in which the concentration variations increase [6, 7, 8, 10]. Figure 7 shows that the nonlinear effects seen in Figure 6 around $t = 1500$ begin when the concentration profiles are tilted by 45°.

Superimposing the concentration field on the relative velocity field (the one seen by an observer travelling with the base flow $\mathbf{w}_0 = q\mathbf{e}_z$), as presented in Figure 8 for $t = 1500$, we observe that the central area, less concentrated, has predominantly upwards velocities, and this region is being fed by low concentration fluid from laterally adjacent tilted regions, indicating that the fluid in the lower concentration layer is

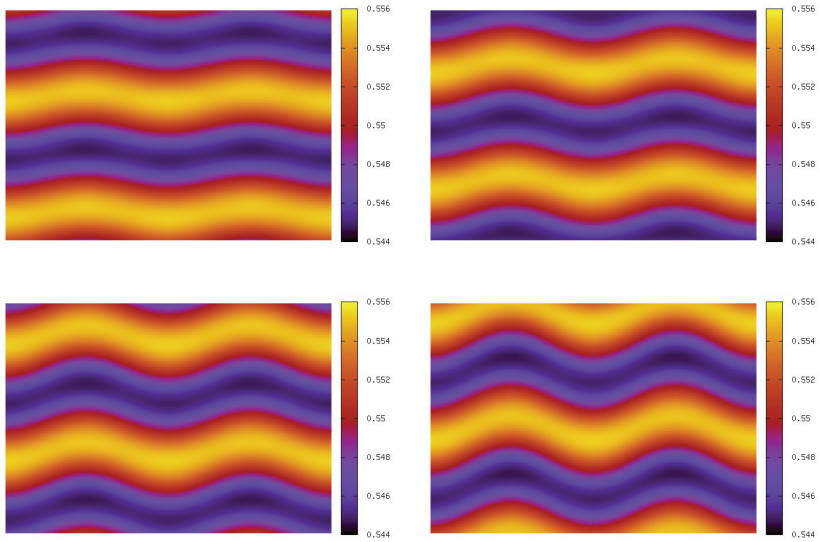

FIG. 7. *Concentration profiles for the simulation presented in Figure* 6. *In the top left picture,* $t = 0$ *and, from left to right, top to bottom,* $t = 641.250$, 1070.625, *and* 1500, *respectively. Two wavelengths in each direction are plotted here.*

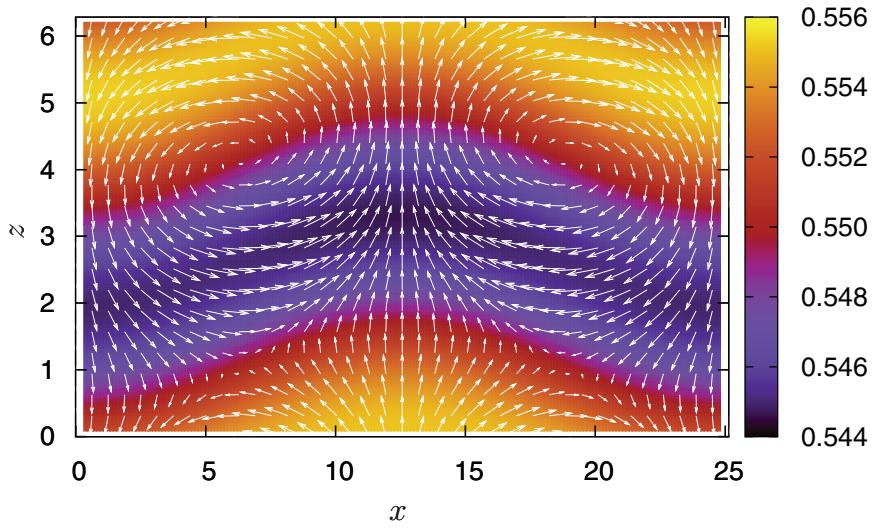

FIG. 8. *Relative velocity field of the disturbances for* $t = 1500$ *superimposed on the particle concentration field. Results for simulation presented in Figure* 6. *One wavelength in each direction is plotted here.*

rising to the peaks of the instabilities. On the other hand, the fluid in the high concentration layer is sliding downwards, moving towards a valley of the instability. In fact, one observes that there are vortical motions located approximately at $x = \pi/2\ell$ and $x = 3\pi/2\ell$, between the low and high concentration layers that are tilting. The intensity of this relative motion increases in time, indicating that the growth

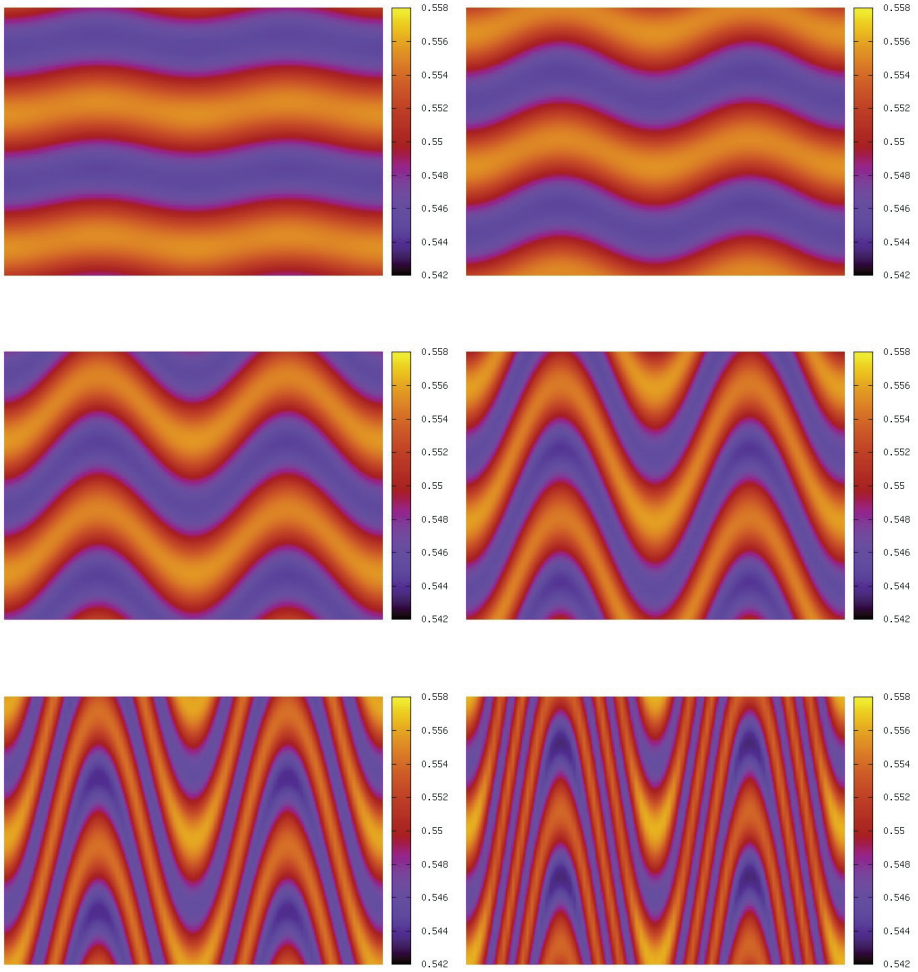

FIG. 9. *Concentration profiles obtained for the simulation presented in Figure* 6. *In the top left picture,* $t = 0$ *and, from left to right, top to bottom, the interval between two consecutive pictures is approximately* 1500 *units of dimensionless times.*

of the instabilities is related to an increase in the tilt of the layers in the unstable configuration. Therefore, we verify with these results the tilt-and-slide mechanism of the gravitational instability, as proposed in [2].

4.3. Comments on nonlinear regimes. Some concentration profiles are plotted for times up to 7500 in Figure 9. As time evolves towards $t = 7500$, the more concentrated fluid flows downwards towards the valleys of the disturbances and accumulates in these regions. Similarly, the less concentrated fluid flows upwards and accumulates in the peaks. As the peaks rise and the valleys descend, the connecting filaments are stretched and squashed together. The squashed concentration profiles eventually hit our numerical resolution, and for this reason we could not proceed beyond $t = 7500$. This region of striations between the peaks and the valleys will behave

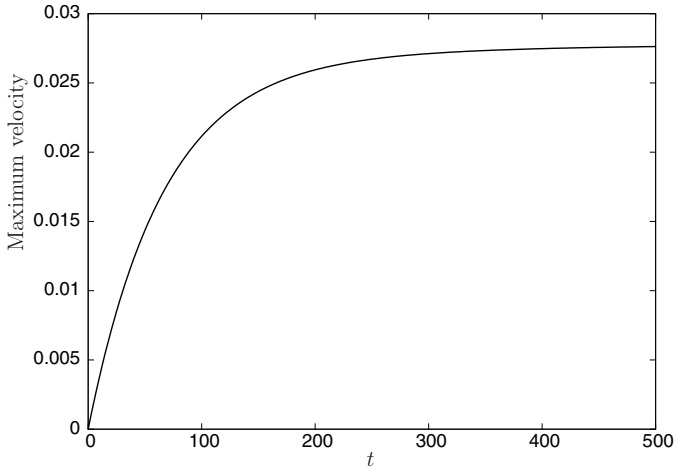

FIG. 10. *Saturation of the maximum velocity of the ascending peaks with respect to time for* $\ell = 0.1$ *and other parameters as in Figure* 6.

as a fluid of the average density. We therefore expect that the velocity of the peaks and valleys will plateau in time in the viscous dominated regime studied here. This can be observed in Figure 10. In our one-fluid model of a fluidized bed, the long time behavior is of the light fluid accumulating near the ascending peaks and the heavy fluid accumulating near the descending valleys. The continually stretched striation joining them act dynamically as a uniform fluid at the mean density. This simple horizontal density variation drives a steady vertical flow.

5. Concluding remarks. In this work, two-dimensional instabilities in a stratified fluid were investigated in order to achieve a better understanding of the dynamics of gravitational overturning. Our first comments concern the analytical results. It was verified that the truncation at $M = 3$ of the approximate analytical solution of (3.14) for the linear stability problem provides an accurate prediction of the growth rates of the secondary instability. This was verified by a numerical calculation of the eigenvalues of (3.14). In addition, the full equations of motion, (2.3), (2.4), and (2.11), were solved numerically using a finite-differences scheme, and the results were validated by their agreement with the predictions of linear theory. With this code, long time nonlinear regimes could be achieved and analyzed.

The growth rates of the secondary instability depend on the amplitude of the stratification. Therefore, the gravitational overturning is more likely to occur in stratification of large amplitudes. This might explain why this kind of instability is more often observed in fluidized beds in which the fluid and the particles have a considerable difference in density (i.e., in gas-fluidized rather than liquid-fluidized beds), since the growth rates of the primary instabilities, responsible for the stratification of the flow in fluidized beds, are then much larger. However, since the model discussed here is not that of a fluidized bed, this may be only partly true.

The secondary instability has proven to be a configurational instability; that is, it does not increase or decrease concentration locally in the flow, but just rearranges the unstable situation of denser fluid over less dense fluid. This is due to the absence of diffusion in the concentration equation, (2.4); that is, particles cannot diffuse from one layer to another. Nevertheless, this is a clear indication that, in the regime studied

here, the expulsion of particles from bubbles in fluidized beds is not connected to a centrifugal expulsion due to the recirculation velocities observed in Figure 8, but might be related to the different rates of filling and emptying of particles of the low concentration regions [5, 15]. We did not see any bubbles in the simulations presented here. In the single-fluid model considered in this work, the particles have no inertia, and so the stratification does not grow from its small initial value. The gravitational overturning, which is proportional to the stratification, is consequently slow. Therefore, in order to address the actual fluidized bed problem, it is important to consider the particles as an independent phase, for which an equation of conservation of momentum is considered, and investigate the effect of inertia of the particles on the flow. We have already started to deal with this issue, and it is still the subject of our current work.

REFERENCES

[1] J. S. Turner, *Buoyancy Effects in Fluids*, Cambridge University Press, Cambridge, UK, 1973.

[2] G. K. Batchelor and J. M. Nitsche, *Instability of stationary unbounded stratified fluid*, J. Fluid Mech., 227 (1991), pp. 357–391.

[3] G. K. Batchelor, *The formation of bubbles in fluidized beds*, in Proceedings of the Symposium Honouring John W. Miles on his 70th Birthday, Ref. Ser. 91, Scripps Institution of Oceanography, San Diego, CA, 1991, pp. 29–44.

[4] R. Jackson, *The Dynamics of Fluidised Particles*, Cambridge University Press, Cambridge, UK, 2000.

[5] S. Sundaresan, *Instabilities in fluidized beds*, in Annu. Rev. Fluid Mech. 35, Annual Reviews, Palo Alto, CA, 2003, pp. 63–88.

[6] T. B. Anderson and R. Jackson, *A fluid mechanical description of fluidized beds: Stability of the uniform state of fluidization*, Indust. Engrg. Chem. Fund., 7 (1968), pp. 12–21.

[7] S. K. Garg and J. W. Pritchett, *Dynamics of gas-fluidized beds*, J. Appl. Phys., 46 (1975), pp. 4493–4500.

[8] G. K. Batchelor, *A new theory of the instability of a uniform fluidized bed*, J. Fluid Mech., 193 (1988), pp. 75–110.

[9] M. Nicolas, J.-M. Chomaz, and E. Guazzelli, *Absolute and convective instabilities of fluidized beds*, Phys. Fluids, 6 (1994), pp. 3936–3944.

[10] K. Anderson, S. Sundaresan, and R. Jackson, *Instabilities and the formation of bubbles in fluidized beds*, J. Fluid Mech., 303 (1995), pp. 327–366.

[11] P. Duru, M. Nicolas, E. J. Hinch, and E. Guazzelli, *Constitutive laws in liquid-fluidized beds*, J. Fluid Mech., 452 (2002), pp. 371–404.

[12] J. Johri and B. J. Glasser, *Connections between density waves in fluidized beds and compressible flows*, AIChE J., 48 (2002), pp. 1645–1664.

[13] B. J. Glasser, I. G. Kevrekidis, and S. Sundaresan, *Fully developed traveling wave solutions and bubble formation in fluidized beds*, J. Fluid Mech., 334 (1997), pp. 157–188.

[14] G. K. Batchelor, *Secondary instability of a gas-fluidized bed*, J. Fluid Mech., 257 (1993), pp. 359–371.

[15] P. Duru and E. Guazzelli, *Experimental investigation on the secondary instability of liquid-fluidized beds and the formation of bubbles*, J. Fluid Mech., 470 (2002), pp. 359–382.

[16] J. J. Derksen and S. Sundaresan, *Direct numerical simulation of dense suspensions: Wave instabilities in liquid-fluidised beds*, J. Fluid Mech., 587 (2007), pp. 303–336.

[17] T. B. Anderson and R. Jackson, *A fluid mechanical description of fluidized beds: Equations of motion*, Indust. Engrg. Chem. Fund., 6 (1967), pp. 527–539.

[18] J. F. Richardson and W. N. Zaki, *Sedimentation and fluidization*, Trans. Inst. Chem. Engineers, 32 (1954), pp. 35–52.